Reversal of Negative Charges on the Surface of *Escherichia coli* Thioredoxin: Pockets versus Protrusions†

Romina Mancusso,‡,⊥ Eduardo Cruz,‡,⊥ Marcela Cataldi,‡ Carla Mendoza,‡ James Fuchs,§ Hsin Wang,# Xiaomin Yang,# and María Luisa Tasayco*,‡

Biochemistry Division, Department of Chemistry, City College of New York, 138th Street and Convent Avenue, New York, New York 10031, Department of Biochemistry, Molecular Biology, and Biophysics, University of Minnesota, 420 Washington Avenue SE, Minneapolis, Minnesota 55455, and Department of Chemistry, College of Staten Island, 2800 Victory Boulevard, New York, New York 10314

Received August 17, 2003; Revised Manuscript Received February 3, 2004

ABSTRACT: Recent studies of proteins with reversed charged residues have demonstrated that electrostatic interactions on the surface can contribute significantly to protein stability. We have used the approach of reversing negatively charged residues using Arg to evaluate the effect of the electrostatics context on the transition temperature (T_m), the unfolding Gibbs free energy change (ΔG), and the unfolding enthalpy change (ΔH). We have reversed negatively charged residues at a pocket (Asp9) and protrusions (Asp10, Asp20, Glu85), all located in interconnecting segments between elements of secondary structure on the surface of Arg73Ala *Escherichia coli* thioredoxin. DSC measurements indicate that reversal of Asp in a pocket (Asp9Arg/Arg73Ala, $\Delta T_m = -7.3$ °C) produces a larger effect in thermal stability than reversal at protrusions: Asp10Arg/Arg73Ala, $\Delta T_m = -3.1$ °C, Asp20Arg/Arg73Ala, $\Delta T_m = 2.0$ °C, Glu85Arg/Arg73Ala, $\Delta T_m = 3.9$°). The 3D structure of thioredoxin indicates that Asp20 and Glu85 have no nearby charges within 8 Å, while Asp9 does not only have Asp10 as sequential neighbor, but it also forms a 5-Å long-range ion pair with the solvent-exposed Lys69. Further DSC measurements indicate that neutralization of the individual charges of the ion pair Asp9-Lys69 with nonpolar residues produces a significant decrease in stability in both cases: Asp9Ala/Arg73Ala, $\Delta T_m = -3.7$ °C, Asp9Met/Arg73Ala, $\Delta T_m = -5.5$ °C, Lys69Leu/Arg73Ala, $\Delta T_m = -5.1$ °C. However, thermodynamic analysis shows that reversal or neutralization of Asp9 produces a 9−15% decrease in ΔH, while both reversal of Asp at protrusions and neutralization of Lys69 produce negligible changes. These results correlate well with the NMR analysis, which demonstrates that only the substitution of Asp9 produces extensive conformational changes and these changes occur in the surroundings of Lys69. Our results led us to suggest that reversal of a negative charge at a pocket has a larger effect on stability than a similar reversal at a protrusion and that this difference arises largely from short-range interactions with polar groups within the pocket, rather than long-range interactions with solvent-exposed charged groups.

Progress in protein engineering depends on our ability to determine the relative significance of hydrophobic and electrostatic contributions to protein folding and stability. While no question remains about the importance of the hydrophobic force in the folding of soluble globular monomeric proteins (*1*), determining the relative importance of electrostatics in protein stability still constitutes a challenge (*2*, *3*). A key event occurred in the 1970s (*4*, *5*) with the appearance of a mesophile of known structure whose homologous thermophilic counterparts exhibited a higher number of ion pairs (*6*). That discovery raised expectations for the untangling of the role of electrostatics on the thermal stability of proteins. The recent explosion of sequence and structural information about these thermophiles (*7*, *8*) has stimulated enormous activity in this area (*2*, *3*, *9*−*11*). Recent computational studies of hyperthermophilic (*12*) and thermophilic (*13*) proteins suggest that thermal stability of these proteins is enhanced by favorable electrostatic interactions arising through the optimum placement of ion pairs. It is known that nature does not always optimize the overall electrostatics of mesophiles for stability (*14*−*17*). In fact, the elegant mutational analysis of cold shock proteins indicates that removal of a pairwise electrostatic repulsion between nearby solvent-exposed charges present in the mesophile but absent in the thermophilic counterpart favors the overall electrostatic interactions and increases stability (*16*). It is thus expected that protein stability could be enhanced by judicious manipulation of the electrostatic interactions among surface residues (*15*, *18*). However, so far de novo engineering of salt bridges in proteins has resulted in only marginal contributions to stability (*19*, *20*), indicating that we are still far from a complete understanding of the contribution of electrostatics to protein stability.

† This work was supported by the RCMI Grant from NIH to C.C.N.Y. and the NSF Grant MCB-0118252 to M.L.T.

* To whom correspondence should be addressed.
⊥ Both authors contributed equally to these studies.
‡ City College of New York.
§ University of Minnesota.
# College of Staten Island.

10.1021/bi0354684 CCC: $27.50
Published on Web 03/11/2004

Recent years have witnessed a great accumulation of experimental and computational studies about electrostatics interactions in peptides and proteins, which, despite stirring some controversy (*21*), have increased our understanding of the significance of salt bridges (*22*−*24*) and long-range electrostatic interactions (*25*) in the folded and unfolded states (*26*) and their contributions to protein stability. Indeed, recent calculations have illuminated experimental studies of the relationship between surface electrostatics and protein stability involving aspects such as ionic strength (*27*), solvent-exposed charges (*28, 29*), ion pairs with different degrees of solvent exposure (*16*, *22*, *28*, *30*−*32*), and charge−charge interactions in the unfolded state (*33*−*39*). In particular, multiple mutational cycles in proteins have been used to assess the charge−charge interactions in ion pairs (*19*, *22*, *40*, *41*) and ion networks (*42*, *43*) on the surface of proteins. More interplay between experimental and computational analysis of electrostatics in proteins (*44*−*47*) is clearly necessary for improving the accuracy of calculated potential energies and the predictive ability needed in protein design and engineering. The purpose of the present mutagenesis studies is to identify patterns in the contributions of negatively charged surface residues to protein stability. We selected to substitute nonconserved negatively charged residues from interconnecting segments of *Escherichia coli* thioredoxin (Trx), a globular monomeric protein of 108 amino acids with a single Arg at position 73, a transition temperature of 86.6 °C, and a negative net charge at neutral pH. The single arginine of Trx was relocated and placed at a pocket (Asp9) or protrusions (Asp10, Asp20, Glu85) of the surface. As it turns out, Asp9 belongs to an ion network of attractive and repulsive long-range ion pairs involving the solvent-exposed Lys69 and Asp10, which makes them likely candidates as important partners. Relocating the Arg of Trx in the pocket produced the most detrimental effect on stability, and therefore Asp9 became the focus of the studies. The possibility that the long-range ion pair Asp9−Lys69 could play an important role led us to include Lys69 in the mutational studies. Our mutational analysis suggest that reversal of a negative charge at a pocket has a larger effect on stability than a similar reversal at a protrusion. This difference, however, arises largely from short-range interactions with polar groups within the pocket rather than long-range interactions with other solvent-exposed charged groups.

MATERIALS AND METHODS

Mutagenesis, Expression, and Purification of Trx Variants. $^{15}NH_4Cl$ was purchased from Cambridge Isotopes Laboratories. All other chemicals were reagent grade. The buffer used in all experiments was 10 mM potassium phosphate (KP_i buffer). Mutations were introduced in the *E. coli* Trx gene carrying the Arg73Ala substitution. Site-directed mutagenesis of this gene was carried out using the QuickChange Site-Directed Mutagenesis kit (Stratagene). The incorporation of the selected mutation was confirmed by DNA sequencing. The plasmid carrying the variant gene was transformed into *E. coli* JF521 (gift from J. Fuchs and C. Woodward) for overexpression (*48*). Each variant was purified to apparent homogeneity by molecular exclusion and reverse phase chromatography (*49*) and subsequently stored in lyophilized form. The lyophilized samples were resuspended in 7 M GuHCl, 10 mM KP_i buffer at pH 7.5. The buffer of each protein sample was exchanged to 10 mM KP_i buffer at pH 7.5 or 6.5 by using a Sephadex G25 column and further concentrated as required. The homogeneity of each protein sample was characterized by SDS/PAGE, analytical reverse phase, analytical gel filtration, and electrospray mass spectroscopy. Uniformly enriched ^{15}N mutants of Trx were obtained by transformation of each plasmid into the *E. coli* BL21 (DE3) strain and subsequent expression in minimal media (*50*). The concentration of each mutant of Trx was determined spectrophotometrically using the average molecular mass and the extinction coefficient $\epsilon_{280} = 14\,100\ M^{-1}\ cm^{-1}$.

Differential Scanning Calorimetry. DSC[1] experiments were performed using a VP-DSC microcalorimeter (MicroCal) with a scan rate of 1.5 deg/min. Samples were filtered and centrifuged at 14 000 rpm previous to the measurements. Calorimetric cells (operating volume ≈ 0.5 mL) were kept under an excess pressure of 207 kPa to prevent degassing during the scan. The reference cell of the calorimeter was filled with KP_i buffer, pH 7.5 from the exchange column. The concentration of the mutants of Trx varied between 0.3 and 1.8 mg/mL. The temperature induced unfolding of all variants were checked for reversibility by comparing the heating and reheating DSC scans. In all cases, the reversibility was better than 75%. The absolute heat capacity, $C_p(T)$, was obtained from the experimentally measured apparent heat capacity difference between the sample cell containing the protein solution and the reference cell containing buffer, $\Delta C_p^{app}(T)$, according to previously published procedures (*49*). The calorimetric profiles were analyzed according to a two-state transition model (*49*). The standard thermodynamic functions under reference conditions were calculated according to the following equations:

$$\Delta C_p^{app}(T) = CV_0\left(C_p(T) - \frac{V_P}{V_{H_2O}}C_{p,H_2O}\right) \quad (1)$$

$$\Delta H_{cal}(T) = \Delta H(T_m) + \Delta C_p(T_m)(T - T_m) \quad (2)$$

$$\Delta S(T) = \Delta S(T_m) + \Delta C_p(T_m)\ln(T/T_m) = \frac{\Delta H_{cal}(T_m)}{T_m} + \Delta C_p(T_m)\ln(T/T_m) \quad (3)$$

$$\Delta G(T) = (T_m - T)\left(\frac{\Delta H_{cal}(T_m)}{T_m} - \Delta C_p(T_m)\right) - T\Delta C_p(T_m)\ln(T/T_m) \quad (4)$$

where C is the protein concentration, V_0 is the volume of the calorimetric cell, V_P and V_{H_2O} are the specific volumes of the protein and water, respectively, T_m is the transition temperature, and $\Delta C_p(T_m)$ is the difference between the absolute heat capacities of the unfolded and folded states of the protein, at the T_m. ΔH, ΔS, and ΔG are, respectively, the changes in enthalpy, entropy, and free energy between the unfolded and folded states.

[1] Abbreviations: CD, circular dichroism; GnHCl, guanidinium hydrochloride; Trx, oxidized *E. coli* thioredoxin; DSC, differential scanning calorimetry; NMR, nuclear magnetic resonance.

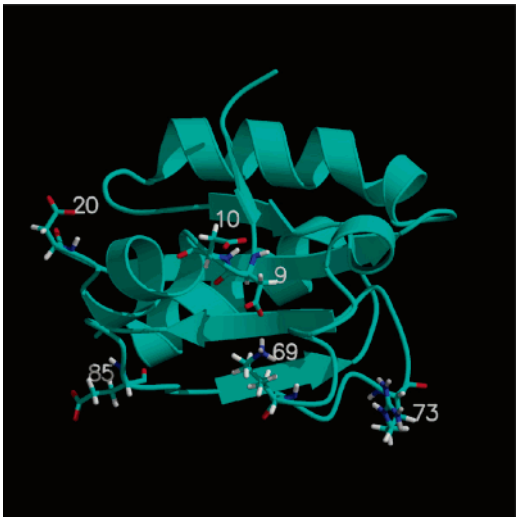

FIGURE 1: Three-dimensional structure of Trx depicting the substitution sites. The figure was generated using the program Molscript (*62*) and rendered with Raster3D (*63*). The hydrogen, nitrogen, and oxygen atoms are shown as white, blue, and red sticks, respectively.

Structural Analysis. Samples containing about 0.3 mM protein in KP_i 90%H_2O/10%D_2O and uncorrected pH 6.5 were prepared and NMR data were acquired on a 600 MHz Varian Unity plus spectrometer at 25 °C. Two-dimensional ^1H-^{15}N HSQC spectra were recorded using eight scans and Fast-HSQC sequence (*51*) with 1024 and 128 complex in t_2, and t_1, respectively. The spectral widths were 8999.9 Hz in the ^1H dimension and 2400 Hz in the ^{15}N dimension. 1D-NMR and 2D-NMR spectra were processed and analyzed on a Silicon Graphics computer using Felix 2.3 (Biosym Technologies, San Diego, CA) and on a Linux machine using NMRPipe (*52*) and NMRView (*53*), respectively.

Structural Calculation. Calculation of the relative burial of different side chains of Trx were performed using the Molmol (*54*) software package for the surface area calculations. Calculations of the electrostatic potentials at the protein surface were carried out using the programs MEAD (*55*) and MSM (*56*). All calculations were performed on the 1xoa.pdb Protein Data Bank entry.

RESULTS

Amino Acid Substitution Sites. Our interest in this subject started when we observed widely different stabilities for some mutants of Trx where the single Arg73 had been relocated to generate proteolytic fragments using arginase. These variants have a charge reversal mutation on surface sites chosen to minimize disruptions of secondary structure: Asp9 and Asp10, which are located between strand β_1 and $helix_1$; Asp20, located between $helix_1$ and β_2; and Glu85, located between β_4 and β_5 (see Figure 1). Our initial observations concerned mutations at positions 9, 20 and 85, and we subsequently extended the studies to Asp10. As it turns out, and it will be important in what follows, Asp9 is located in a pocket while the others are in protrusions (see Figure 2). Asp9 is therefore much less exposed and surrounded by more heavy atoms than the other three (see Table 1), making short-range interactions with nonpolar (Phe12, Gly65) and polar (Asn63, Thr66, Lys69) residues. An interesting observation from the 3D structure of Trx is that the oxygen of the carboxylate of Asp9 is in the middle of an ionic network: it is about 5 Å from the nitrogen of the amino of Lys69 and 6 Å from the oxygen of the carboxylate of Asp10 (see Figures 1 and 2). Since preliminary thermal denaturation experiments of the variants using increasing concentrations of NaCl (0−1 M) and far-UV CD spectroscopy exhibited only subtle shifts in the unfolding transition (data not shown), which is not necessarily unexpected (see ref *47* and references therein), we decided to evaluate the role of the electrostatic interaction between Asp9 and Lys69 by neutralization of the individual charges at positions 9 and 69 using nonpolar, or moderately nonpolar, residues. These residues were judiciously chosen to be of similar size to the charged residues in question: Ala for Asp, Met for Arg, and Leu for Lys. For technical reasons related to the generation of proteolytic fragments of *E. coli* Trx, all the charge reversal mutations were carried out on a mutant of Trx whose Arg73 was replaced by Ala (Arg73Ala). Therefore, all comparisons are made with respect to this mutant.

Effect of Amino Acid Substitution on the Folded State of the Trx Variants. Size exclusion chromatography of Arg73Ala Trx and its variants indicates a similar elution volume (data

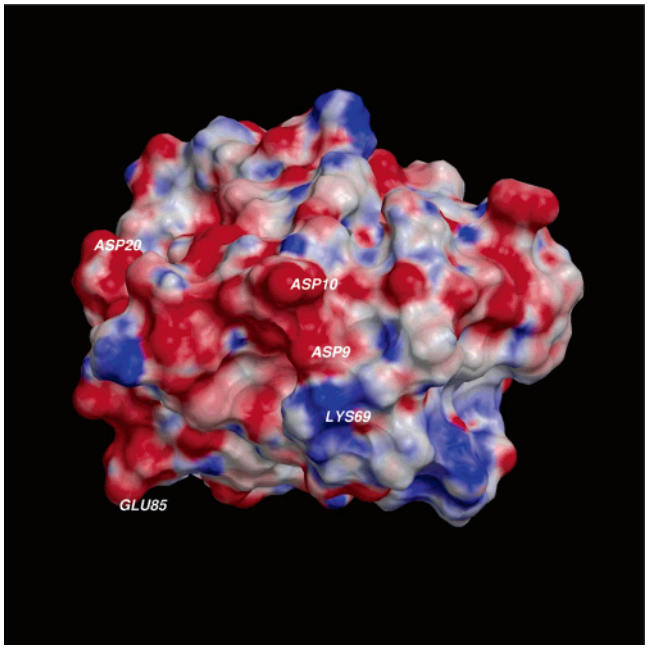

FIGURE 2: Electrostatic potential at the surface of *E. coli* Trx. The potential was generated using the program MEAD (*55*); the surface was generated with the MSM program (*56*); the final picture was created with the program DINO (http://www.dino3d.org) and rendered with Raster3D (*63*). The negative and positive charges are depicted in blue and red, respectively.

Table 1: Solvent Exposure (in Å^2) and Number of Heavy Atoms within a 7-Å Radius Surrounding Selected Charged Residues from *E. coli* Trx[a]

residue	ΔASA	ΔASA (%)	no. of neighbors
Asp9	52.1	21.6% of 240.9	174
Asp10	127.6	52.2% of 244.2	81
Asp20	134.0	56.8% of 235.8	55
Lys69	125.9	43.0% of 293.0	166
Arg73	181.9	57.5% of 316.2	138
Glu85	125.9	47.6% of 264.3	102

[a] Surface exposures were computed using the program Molmol (*54*) and correspond to the average of the 20 structures present in the 1Xoa.pdb Protein Data Bank Entry

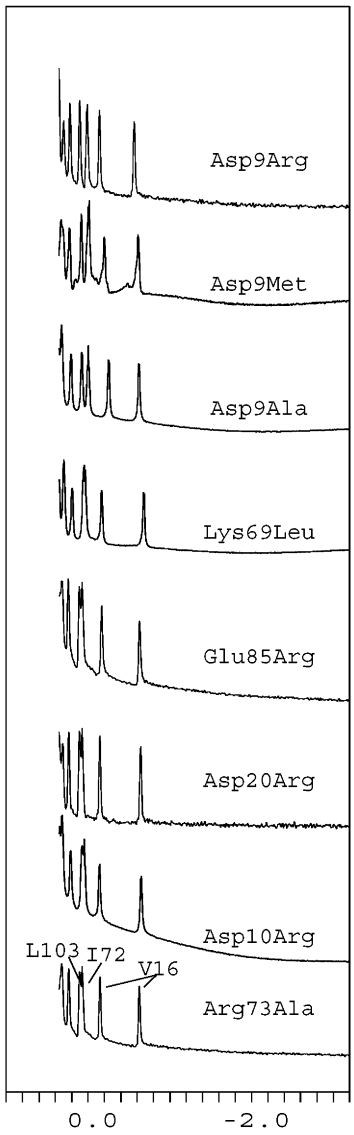

FIGURE 3: Overlay of upfield portion of the 1D-NMR spectrum of single and double variants of *E. coli* Trx: Arg73Ala, Asp10Arg, Asp20Arg, Glu85Arg, Lys69Leu, Asp9Ala, Asp9Met, Asp9Arg. Assignments are indicated on Arg73Ala.

not shown), implying that these substitutions do not alter the monomeric state of Trx. Comparing the upfield portion of the 1D-NMR spectrum for Arg73Ala Trx with that of its variants indicates that substitutions at position 9 increase the separation between the peaks of Ile72 and Leu103 and decrease the distance between the two peaks of Val16 (*57*) (see Figure 3). The peaks of Ile72 and Leu103 also show a better overlap in the spectrum of Lys69Leu than that of Arg73Ala. On the basis of previous assignments of Trx (*58*), the ^{15}N-^{1}H-HSQC spectra of the double variants, i.e., Asp9Arg, Asp20Arg, and Glu85Arg show shifted cross-peaks with respect to that of Arg73Ala Trx for amide protons of residues in the vicinity of the substitution site (see Figure 4). For instance, the spectrum of Asp20Arg and Glu85Arg (data not shown) exhibits subtle shifts only in the vicinity of the substitution site. However, Asp9Arg shows a more pronounced effect, which includes residues located within the 5 Å radius, i.e., Phe12, Asn63, Gly65, Thr66, Lys69 and residues beyond the 5 Å radius such as Val16, Phe27, Ala67, Ile72. These results reflect conformational changes in the

Table 2: Effects of Amino Acid Substitutions on the Thermodynamic Parameters of Unfolding Trx[a]

variant[b]	T_m (°C)[c]	ΔH (T_m) (kJ/mol)	ΔC_p (T_m) (kJ/K mol)	ΔH (82 °C) (kJ/mol)	$\Delta\Delta G$ (82 °C) (kJ/mol)
Asp9Arg	78.2	338.0 ± 0.6	6.3 ± 0.2	361	−8.11
Asp9Met	80.1 ± 0.2	344.3 ± 0.5	4.8 ± 0.2	352	−6.23
Lys69Leu	80.4	427.1 ± 0.2	7.3 ± 0.7	437	−6.34
Asp9Ala	81.8	386.4 ± 0.4	5.5 ± 0.1	386	−4.48
Asp10Arg	82.4	429.3 ± 0.4	7.0 ± 0.1	426	−3.9
Arg73Ala	85.5	456.2 ± 0.3	7.5 ± 0.1	424	0[e]
Asp20Arg	87.5	452.2 ± 0.4	7.6 ± 0.4	414	+1.77
Glu85Arg	89.4	458.5 ± 0.5	5.9 ‡	415	+4.53

[a] Transition temperatures (T_m), unfolding enthalpy change (ΔH), unfolding heat capacity change (ΔC_p), and unfolding free energy change (ΔG) were derived from the two-state fittings to DSC profiles of the variants at a range of concentrations spanning 0.3−1.8 mg/mL in KP_i buffer, pH 7.5. Standard errors and uncertainty associated with the ΔH, ΔC_p, and ΔG are estimated from the scatter of values corresponding to independent DSC measurements. [b] With the exception of Arg73Ala, all the variants are double mutants that contain the Arg73Ala mutation. Van't Hoff ratios of all the variants are close to 0.99. [c] Except when noted the errors are less than 0.1 °C. [d] Calculated according to the theoretical model of Freire et al. (*61*). [e] The ΔG at 82 °C is +4.51 kJ/mol.

N-terminal portion of helix$_1$ and β_4, the C-terminal portion of β_2 and β_5, as well as the long interconnecting segment between β_3 and β_4. Together, the NMR analysis demonstrates that substituting Asp9 produces extensive conformational changes on an area close to the disulfide Cys32−Cys35 (see Figure 5). As expected, the far and near-UV CD analysis indicates minimal changes in the content of secondary and tertiary structure of all the variants with the exception of Asp9Arg, whose near-UV spectrum shows a subtle difference that may arise from perturbations of Trp28, Trp31, and Tyr70 (data not shown).

Effect of Amino Acid Substitutions on the Thermostability. The analysis of at least three sets of reversible DSC experiments of the variants of Trx at concentrations between 0.3 and 1.8 mg/mL (see Figure 6) provides, under the assumption of a two-state process, a complete set of thermodynamic parameters (see Table 2). The fitting of the DSC measurements is excellent and yields Van't Hoff ratios close to unity, implying that the two-state assumption is warranted. Interestingly, the charge reversal in the pocket produces a decrease in T_m of about 7 °C, while the reversals at the protrusions can go either way but by not more than 2−4 °C. Interestingly, this includes Asp10, whose carboxylate is within 5.9 Å of Asp9. The pronounced drop in the case of the pocket led us to investigate the potential electrostatic interaction partners of Asp9 (see Figure 2), of which the most prominent is Lys69 (charged moieties are within 5.1 Å). Neutralization of Asp9 by an Ala or Met decreases the T_m by 4 and 5 °C, respectively. The small difference between the Ala and Met mutations seems to indicate that the effect of elongating the nonpolar side chain is not more than 2 °C. Moreover, neutralization of Lys69 produces a drop of 5 °C. Thus, neutralization of either residue in the Asp9−Lys69 pair exhibits similar effects in the ΔG and T_m. However, as we will see, the picture is dramatically different when one looks at the changes in ΔH.

Effect of Amino Acid Substitutions on the Enthalpies of Unfolding. The next step is to compare the enthalpy of unfolding of the Trx variants at a reference temperature of

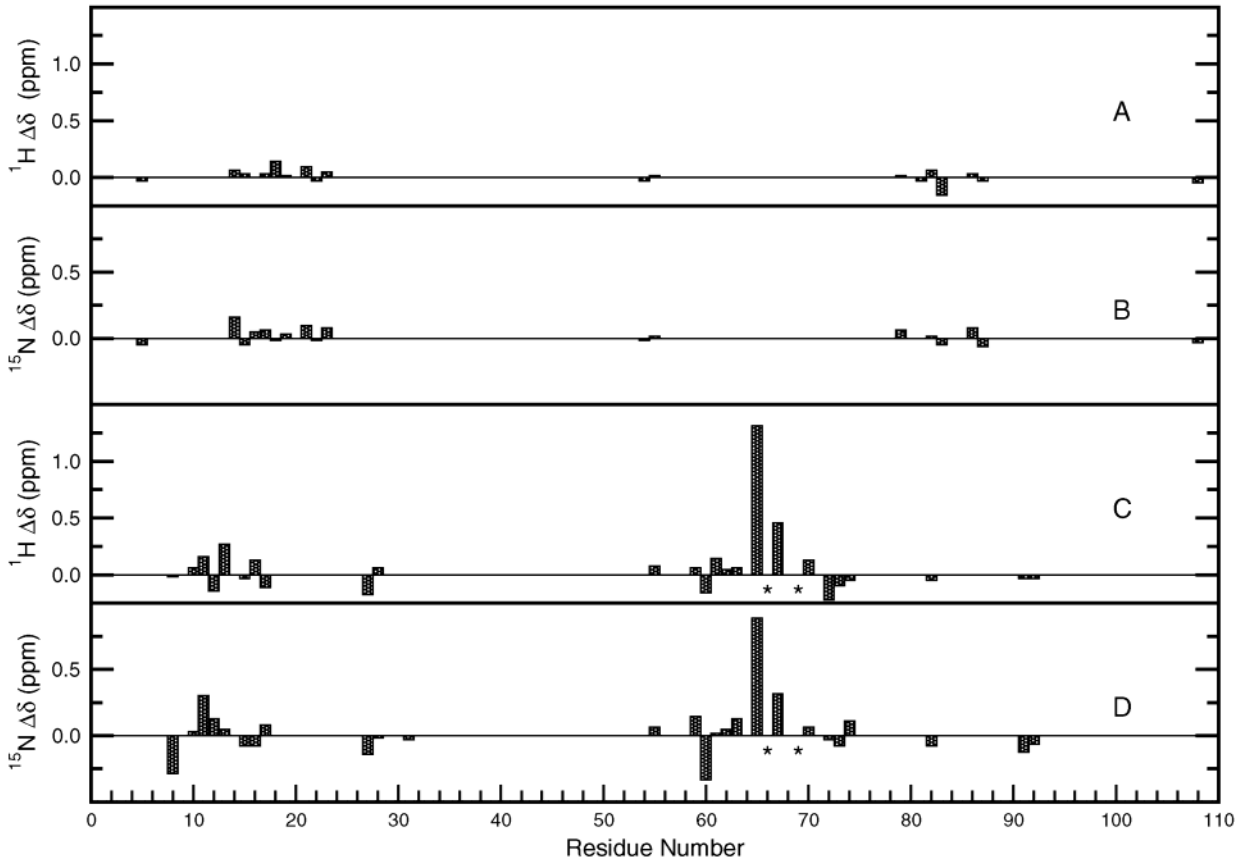

FIGURE 4: Plots of the observed chemical shift values for the amide protons and nitrogens of a ^{15}N-labeled double variant of *E. coli* Trx minus that of Arg73Ala Trx. (A) Δδ (in ppm) for amide protons of double variant Asp20Arg. (B) Δδ (in ppm) for amide nitrogens of double variant Asp20Arg. (C) Δδ (in ppm) for amide protons of double variant Asp9Arg. (D) Δδ (in ppm) for amide nitrogens of double variant Asp9Arg. Residues 66 and 69 were shifted, but their shifts were undetermined and they are marked with an asterisk in the figure.

FIGURE 5: Three-dimensional structure of Trx. The network of residues showing changes in chemical shifts of the amide protons upon replacement of Asp9 by Arg are depicted in shades of blue. A selected subset of the side chains has also been depicted and labeled to show direct and indirect interactions with Asp9. The figure was generated using the program Molscript (*62*) and rendered with Raster3D (*63*).

82 °C, an average transition temperature that minimizes the errors of extrapolation due to the temperature dependence of ΔC_p (see Table 2). The differences in ΔH of unfolding between the variants with substitutions at position 9 and the remaining variants are beyond the expected errors associated with protein concentration measurements. For instance, a 5% decrease in the concentration of Asp9Arg translates in a 1% increase in the ΔH value at the T_m and a 2.8 and 6.7% increase in the ΔH and ΔG values of unfolding, respectively, at 82 °C. On the basis of the ΔH values, two groups of variants are clearly defined: (i) those arising from a reversal of a charge at protrusions, including Asp10, which show essentially the same enthalpy of unfolding found for Arg73Ala (between 413 and 426 kJ/K·mol) and a T_m above 82 °C, and (ii) those corresponding to the neutralization or reversal of the negatively charged Asp9 sitting in a surface pocket, which produce a drop in the ΔH (to a value between 352 and 386 kJ/K·mol) and have a T_m below 82 °C. One interesting exception is the solvent-exposed Lys69Leu: the ΔH is similar to that of Arg73Ala, but the T_m is lower than 82 °C. Since the Gibbs free energy of unfolding (ΔG) of the variants at 82 °C exhibits the same trend as the thermostability (see Table 2), these two groups of variants can be also organized by the ΔG values.

Summary. The mutations we have studied seem to indicate that reversal of Asp9 at the pocket is the most detrimental to stability. Moreover, only the replacement of Asp9 at the pocket affects the ΔH to any significant degree. Interestingly, a reduction in the ΔH occurs irrespective of whether the replacement is a polar (Arg) or nonpolar (Ala, Met) residue and is accompanied by the propagation of structural changes to distant residues (beyond 9 Å). In fact, this is the only case in which such structural changes are observed, which is consistent with our expectation that structural changes result in changes in ΔH.

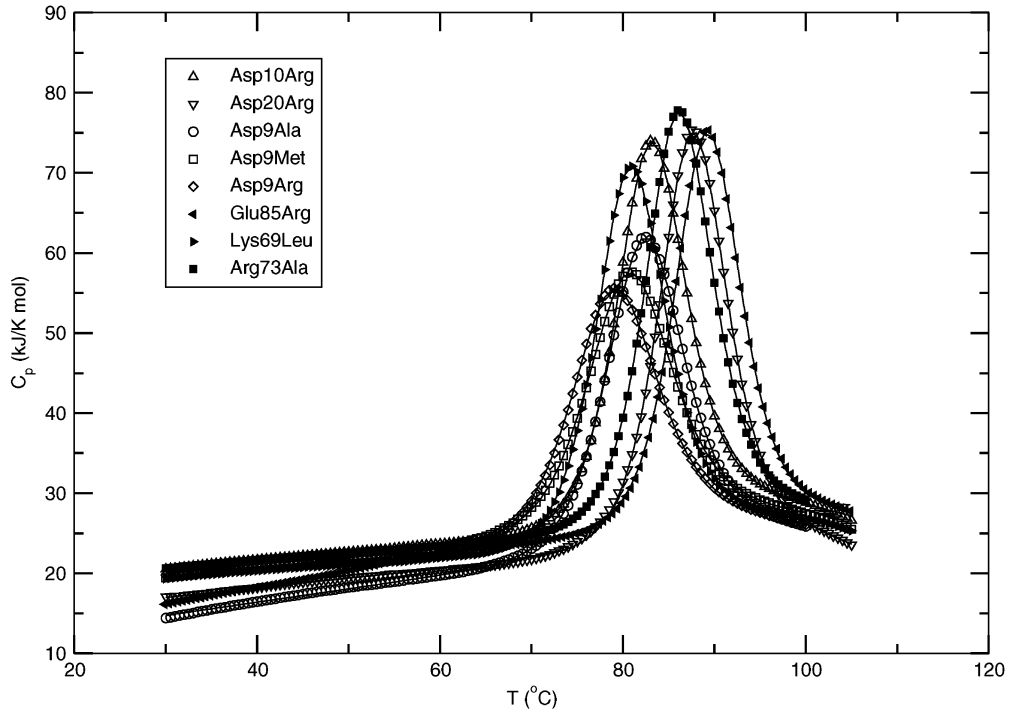

FIGURE 6: Temperature dependence of the absolute heat capacity of the double variants of *E. coli* Trx obtained by DSC measurements. The results of the data analysis are shown in symbols, and the best fits to the two-state equilibrium model are shown as continuous lines.

DISCUSSION

Structure and Energetics of Substitutions at Protrusions. Structural analysis at low (far and near-UV CD) and high (1D-NMR and $^1H^{15}N$-HSQC) resolution of the variants with reversal of charge at the protrusions shows that, overall, they maintain the structure of Trx.

As far as the energetics, Glu85Arg is the most stable variant, regardless of whether one compares the ΔG or the T_m (see Table 2). Assuming that the nonpolar portion of the long side chain of Arg arranges itself according to the interactions of the guanidinium, the increasing trend in stability going from Asp10Arg to Asp20Arg, and Glu85Arg reflects differences in the polar/electrostatic context around the Arg in these protrusions. In all these cases, the ΔH at the reference temperature are the same, within the experimental uncertainties (3%), and it is not clear whether the differences in the polar/electrostatic context have any effect on the enthalpies. It is, however, provocative to believe that the increase in stability relative to Arg73Ala shown by the solvent-exposed Asp20Arg and Glu85Arg arises from entropic contributions. Indeed, recent computational studies indicate that the long Arg side chain shields the backbone from solvation and contributes entropically to the increase of stability (*24*). On the other hand, Asp10Arg shows a decrease in the unfolding ΔG of about 3.9 kJ/mol relative to Arg73Ala and also exhibits a clear difference in context: the carboxylate oxygens of Asp10 and Asp9 are within 6 Å from each other, but both Asp20 and Glu85 are at least 8 Å away from any nearby charge. This reflects the complexity of the ionic network around Asp10 and awaits further mutational analysis.

In summary, the reversal of a negative charge at protrusions affects the T_m either way (by not more than 2−4 °C), and produces almost no structural changes and negligible changes in ΔH.

Structure and Energetics of Substitutions at the Pocket. Analysis of the 1D-NMR spectra of the family of variants with substitutions at position 9 (see Figure 3) shows shifts in the methyl group of either Ile72 or Leu103, and the $^1H^{15}N$-HSQC (see Figure 4) spectrum of variant Asp9Arg shows a change in the amide of Ile72 and not in that of Leu103. We therefore conclude that, regardless of their polarity and size (Ala, Met, or Arg), substitutions at position 9 produce conformational changes of Ile72, which lies beyond the 5-Å radius. From the HSQC spectrum of Asp9Arg, we can also see changes, although subtle, in Phe12 and Phe27, and therefore it is likely that the change in Ile72 stems from a direct interaction between Asp9 and Phe12. It is worth noting that Phe12 and Ile72 are connected through at least two hydrophobic networks of native Trx: Phe12−Phe27−Ile72 (see Figure 5) and Phe12−Phe27−Ala67−Ile72. Structural perturbations are also found on Gly65, Thr66, Lys69, which appear to reflect other native networks of interactions: Asp9−Lys69, Asp9−Gly65−Lys69, Asp9−Thr66−Lys69, Asp9−Phe12−Thr66−Lys69, and Asp9−Phe12−Phe27−Thr66−Lys69. These structural perturbations demonstrate that substitution of Asp9 at the pocket produces extensive conformational changes in the surroundings of solvent-exposed Lys69 (see Figure 5) and, most importantly, demonstrate the existence of direct and indirect routes of interaction between Asp9 and Lys69. On the other hand, neutralization of Lys69 (Lys69Leu) shows no structural changes. Unfortunately, the asymmetry in these structural perturbations complicates the use of the elegant double mutagenesis approach (*47*, *59*, *60*) to extract information about the effect of the putative long-range ion pair Asp9−Lys69.

The variants with substitutions of Asp9 at the pocket not only exhibit the largest conformational changes, but also the largest decrease in the ΔH of unfolding (9−15%, see Table

2). An important question is whether experimental errors account for this drop; in particular, we wanted to know whether these results are sensitive to errors in the protein concentration, which is one of the least reliable measurements. We therefore evaluated the impact of a 5% error in concentration of Asp9Arg and found that it results in only a 3% error in the ΔH at the reference temperature. Another source of errors could be the fact that the unfolded baselines of the most stable variants are much shorter than the folded ones (see Figure 6), and therefore the resulting ΔC_p at T_m may be inaccurate. The dispersion in the ΔC_p at the T_m does not, however, affect the ΔH values at the T_m. At this point, the only remaining question is about the effect of errors arising from the temperature dependence of the ΔC_p. In this regard, the reference temperature was selected as the median of the T_m values to minimize the errors due to extrapolation. We therefore conclude that the extensive structural perturbations of the variants with substituents of Asp9 at the pocket produce a real and significant decrease in the ΔH of unfolding.

Disruption of Electrostatic Interactions Inside the Pocket Drives the Decrease in ΔH. The decrease in the ΔG and T_m upon neutralization of Asp9 by Ala indicates that removal of the carboxylate from this pocket costs 4.5 kJ/mol and near 4 °C. Further decrease upon replacing Ala by Met suggests that extending the methylene chain out of the pocket costs 1.8 kJ/mol and almost 2 °C. Assuming that Met and Arg have similar nonpolar effects, introducing a positive charge is worth 1.9 kJ/mol and about 2 °C. Thus, if we dissect the decrease in ΔG (8.2 kJ/mol) and T_m (7 °C) observed in Asp9Arg into contributions arising from neutralization (4.5 kJ/mol and near 4 °C), elongation of side chain (1.8 kJ/mol and almost 2 °C), and ionization with opposite charge (1.9 kJ/mol and about 2 °C), neutralization stands out as the most prominent effect. Indeed, recent experiments (data not shown) show that replacing Asp9 by Asn has the same effect as replacement by Met (decrease in ΔG and ΔH), confirming that the removal of the carboxylate from the pocket at position 9 has the most detrimental effect on stability (4.5−6.2 kJ/mol and about 4−5 °C).

Interestingly, the neutralization of Asp9 (Ala, Met) decreases the ΔH value by about 38 kJ/mol, but the replacement of a nonpolar side chain at the same position by a charged one (Met to Arg) does not further affect the ΔH value (see Table 2). Thus, it seems that the cost of neutralizing Asp9 at a pocket is independent of the side chain length, and the ionization with an opposite charge of a long nonpolar side chain (Met to Arg) reaching out of that pocket has just an entropic effect, that is, the change in ΔG is mostly due to a change in ΔS.

Assuming that the nonpolar interactions involving Lys69 are similar to the ones for Leu, the decrease in ΔG and T_m of Lys69Leu implies that this neutralization costs 6.3 kJ/mol and 5 °C. It seems therefore that the loss of stability due to individual neutralization of the solvent-exposed Lys69 and Asp9 at a pocket is about the same. A naive interpretation of these results is that the long-range attractive ion pair Asp9−Lys69 has a significant stabilizing effect. However, the lack of change in ΔH upon neutralization of one of the partners, Lys69, implies that the decrease in ΔG for this particular neutralization is rather entropic (*24*). This fact makes the naive interpretation less believable, since changes

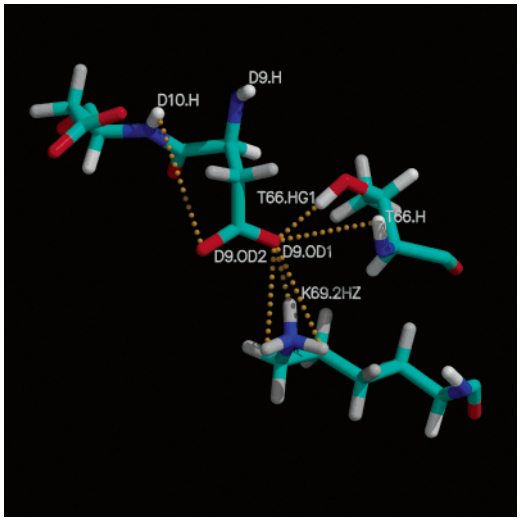

FIGURE 7: Close-up of the three-dimensional structure of Trx depicting the residues with charged and polar side chains within 5 Å of Asp9. Some of the possible electrostatic interactions with the carboxylate of Asp9 are depicted with broken lines. Color coding: red: O; blue: N; gray: H; green: C. The figure was generated using the program Molscript (*62*) and rendered with Raster3D (*63*).

in the values of both ΔG and ΔH are expected whenever a long-range ion pair plays a significant role in stability. It is possible that compensatory favorable enthalpic contributions result in the same ΔH, but this is unlikely because no significant structural changes are found, just as for the other solvent exposed charges studied here (Asp20, Glu85, and Arg73). This led us to find other electrostatic interactions with low sensitivity to ionic strength that may be responsible for the decrease in ΔH upon substitution of Asp9 at a pocket. We thus conclude that this decrease is driven by (electrostatic) short-range interactions with polar groups within the pocket, that is, with the amide and hydroxyl protons of buried Thr66, rather than long-range interactions with the solvent-exposed Lys69 (see Figure 7). These results are surprising considering that the recent work of Raleigh and co-workers (*47*) implies that salt bridge effects become more significant as the surface salt bridge becomes more buried, while our results suggests that short-range electrostatic interactions begin to predominate in those cases.

Many simplified models have been used to calculate charge−charge interactions on protein surfaces. Indeed, calculations of the charge−charge interactions of Trx using a variant of the Tanford-Kirkwood model (*19*, *20*), in which the protein surface is treated as a smooth sphere but some corrections for solvent accessibility are made, indicate, in increasing order, that Glu85, Asp20, Asp9, and Asp10 are involved in destabilizing charge−charge interactions, while Arg73 and Lys69 are involved in stabilizing charge−charge interactions. Interestingly, these calculations support the subtle reduction in thermostability of Arg73Ala relative to Trx (T_m = 86 °C) and the further decrease of that for the double variant Lys69Leu. They are also consistent with the enhanced thermostability of the double variants Asp20Arg and Glu85Arg, although not in the appropriate order. However, they fail to account for the decrease in the thermostability of the double variant Asp9Arg, which is not unexpected if, as we believe, the determining factors are the short-range interactions with polar groups within the pocket rather than long-range interactions with solvent-exposed

charged groups. Thus, more experimental analysis of electrostatics in proteins is clearly necessary as benchmarks for computational analysis to improve the predictive ability of protein design.

CONCLUDING REMARKS

Our results demonstrate that charge reversal of Asp at protrusions results in changes in stability that are mainly of entropic origin, that is, the changes in ΔG are due to changes in ΔS, while ΔH remains unaffected within the experimental errors. On the other hand, substitutions of Asp9 at a pocket produces extensive conformational changes, significant (9−15%) decreases in ΔH, and significant effects in ΔG. In fact, the most detrimental decrease in stability arises from the reversal of Asp9 at a pocket, and this can be dissected into contributions from neutralization (4.5 kJ/mol and near 4 °C), elongation of the neutral side chain (1.8 kJ/mol and almost 2 °C), and ionization with opposite charge (1.9 kJ/mol and about 2 °C). In regard to the ionic partners of Asp9, neither charge reversal of Asp10 at a protrusion nor neutralization of the solvent-exposed Lys69 show extensive conformational changes, or changes in ΔH, indicating that the long-range interactions of Asp9 at a pocket with solvent-exposed charged groups are not the dominant contributions.

Our results led us to suggest that reversal of a negative charge at a pocket has a larger effect on stability than a similar reversal at a protrusion and that this difference arises largely from short-range interactions with polar groups within the pocket, rather than long-range interactions with solvent-exposed charged groups.

ACKNOWLEDGMENT

We thank Angel García and Francisco Figueirido for helpful discussions. We also thank José Sánchez-Ruiz, Themis Lazaridis, and Marilyn Gunner for their comments, and the MLTJ's lab for their involvement in mutagenesis (Elva Paredes, Alexandra Obregón, and Roxana Georgescu), expression (Martin Indarte, Elva Paredes, and Marcela Herrera), purification (Marcela Herrera), and NMR spectroscopy (Vilma Arriarán, Carla Rospigliosi, Martin Indarte, and Mario Pujato) of the Trx variants.

REFERENCES

1. Dill, K. A. (1990) Dominant forces in protein folding. *Biochemistry 29*, 7133.
2. Kumar, S., and Nussinov, R. (1999) Salt bridge stability in monomeric proteins. *J. Mol. Biol. 293*, 1241.
3. Kumar, S., and Nussinov, R. (2002) Close-range electrostatic interactions in proteins. *ChemBioChem 3*, 604.
4. Perutz, M. F., and Raidt, H. (1975) Stereochemical basis of heat stability in bacterial ferredoxins and in haemoglobin a2. *Nature 255*, 256.
5. Perutz, M. F. (1978) Electrostatic effects in proteins. *Science 201*, 1187.
6. Barlow, D. J., and Thornton, J. M. (1983) Ion pairs in proteins. *J. Mol. Biol. 168*, 867.
7. Kumar, S., Tsai, C.-J., and Nussinov, R. (2000) Factors enhancing protein thermostability. *Protein Eng. 13*, 179.
8. Kumar, S., and Nussinov, R. (2001) How do thermophilic proteins deal with heat? *Cell. Mol. Life Sci. 9*, 1216.
9. Kumar, S., and Tsai, C.-J. (2001) Thermodynamic differences among homologous thermophilic and mesophilic proteins. *Biochemistry 40*, 14152.
10. Kumar, S., and Nussinov, R. (2002) Relationship between ion pairs geometries and electrostatic strengths in proteins. *Biophys. J. 3*, 1595.
11. Kumar, S., and Nussinov, R. (2001) Ion pairs and their stabilities fluctuate in NMR conformers ensembles of proteins. *Proteins 43*, 433.
12. Xiao, L., and Honig, B. (1999) Electrostatic contribution to the stability of hyperthermophilic proteins. *J. Mol. Biol. 289*, 1435.
13. Kumar, S., Ma, B., Tsai, C.-J., and Nussinov, R. (2000) Electrostatic strengths of salt bridges in thermophilic and mesophilic glutamate dehydrogenase monomers. *Proteins 38*, 368.
14. Ibarra-Molero, B., Loladze, V. V., Makhatadze, G. I., and Sánchez-Ruiz, J. M. (1999) Thermal versus guanidine-induced unfolding of ubiquitin. An analysis in terms of the contributions from charge−charge interactions to protein stability. *Biochemistry 38*, 8138.
15. Loladze, V. V., Ibarra-Molero, B., Sánchez-Ruiz, J. M., and Makhatadze, G. I. (1999) Engineering a thermostable protein via optimization of charge−charge interactions on the protein surface. *Biochemistry 38*, 16419.
16. Perl, D., and Schmid, F. X. (2001) Electrostatic stabilization of a thermophilic cold shock protein. *J. Mol. Biol. 313*, 343.
17. Langsetmo, K., Fuchs, J. A., and Woodward, C. K. (1991) The conserved, buried aspartic acid in oxidized *E. coli* thioredoxin has a pK_a of 7.5. Its titration produces a related shift in global stability. *Biochemistry 30*, 7603.
18. Sánchez-Ruiz, J. M., and Makhatadze, G. I. (2001) To charge or not to charge. *Trends Biotech. 19*, 132.
19. Sali, D., Bycroft, M., and Fersht, A. R. (1991) Surface electrostatic interactions contribute little to stability of barnase. *J. Mol. Biol. 220*, 779.
20. Sánchez-Ruiz, J. M., personal communication.
21. Hendsch, Z. S., and Tidor, B. (1994) Do salt bridges stabilize proteins? A continuum electrostatic analysis. *Protein Sci. 3*, 211.
22. Tissot, A. C., Vuilleumier, S., and Fersht, A. R. (1996) Importance of two buried salt bridges in the stability and folding pathway of barnase. *Biochemistry 35*, 6786.
23. Olson, C. A., Spek, E. J., Shi, Z., Vologodskii, A., and Kallenbach, N. R. (2001) Cooperative helix stabilization by complex Arg-Glu salt bridges. *Proteins: Struct. Funct. Genet. 44*, 123.
24. Ghosh, T., Garde, S., and García, A. E. (2003) Role of backbone hydration and salt bridge formation in stability of α-helix in solution. *Biophys. J. 85*, 3187.
25. Grimsley, G. R., Shaw, K. L., Fee, L. R., Alston, R. W., Huyghues-Despointes, B. M. P., Thurlkill, R. L., Scholtz, J. M., and Pace, C. N. (1999) Increasing protein stability by altering long-range coulombic interactions. *Protein Sci. 8*, 1843.
26. Oliveberg, M., Arcus, V. L., and Fersht, A. R. (1995) pK_a values of carboxyl groups in the native and denatured states of barnase: The pK_a values of the denatured state are on average 0.4 units lower than those of model compounds. *Biochemistry 34*, 9424.
27. Dominy, B. N., Perl, D., Schmid, F. X., and Brooks, C. L., III (2002) The effects of ionic strength on protein stability: The cold shock protein family. *J. Mol. Biol. 319*, 541.
28. Dong, F., and Zhou, H.-X. (2002) Electrostatic contributions to T4 lysozyme stability: solvent exposed charges versus semi-buried salt bridges. *Biophys. J. 83*, 1341.
29. Sun, D.-P., Soderlind, E., Baase, W. A., Wozniak, J. A., Sauer, U., and Matthews, B. W. (1991) Cumulative site-directed charge−charge replacement in bacteriophage T4 lysozyme suggest that long-range electrostatic interactions contribute little to protein stability. *J. Mol. Biol. 221*, 873.
30. Anderson, D. E., Becktel, W. J., and Dahlquist, F. W. (1990) pH-induced denaturation of proteins: A single salt bridge contributes 3−5 kcal/mol to the free energy of folding of T4 lysozyme. *Biochemistry 29*, 2403.
31. Vijayakumar, M., and Zhou, H.-X. (2001) Salt bridges stabilize the folded structure of barnase. *J. Phys. Chem. 105*, 7334.
32. Zhou, H.-X., and Dong, F. (2003) Electrostatic contributions to the stability of a thermophilic cold shock protein. *Biophys. J. 84*, 2216.
33. Zhou, H.-X. (2003) Direct test of the Gaussian-chain model for treating residual charge−charge interactions in the unfolded state of proteins. *J. Am. Chem. Soc. 125*, 2060.
34. Whitten, S. T.; García-Moreno, E. B. (2000) pH dependence of stability of staphiloccal nuclease: Evidence of substantial electrostatic interactions in the denatured state. *Biochemistry 39*, 14292.

35. Zhou, H.-X. (2002) Residual charge interactions in unfolded staphylococcal nuclease can be explained by the Gaussian-chain model. *Biophys. J. 83*, 2981.
36. Zhou, H.-X. (2002) Residual electrostatic effects in the unfolded state of the N-terminal domain of L9 can be attributed to nonspecific nonlocal charge−charge interactions. *Biochemistry 41*, 6533.
37. Oliveberg, M., Vuilleumier, S., and Fersht, A. R. (1994) Thermodynamic study of the acid denaturation of barnase and its dependence on ionic strength: Evidence for residual electrostatic interactions in the acid/thermally denatured state. *Biochemistry 31*, 2728.
38. Guzmán-Casado, M., Parody-Morreale, A., Robic, S., Marqusee, S., and Sánchez-Ruiz, J. M. (2003) Energetic evidence for formation of a pH-dependent hydrophobic cluster in the denatured state of Thermus thermophilus ribonuclease H. *J. Mol. Biol. 329*, 731.
39. Horng, J. C., Moroz, V., Rigotti, D. J., Fairman, R., and Raleigh, D. P. (2002) Characterization of large peptide fragments derived from the N-terminal domain of the ribosomal protein L9: Definition of the minimum folding motif and characterization of local electrostatic interactions. *Biochemistry 41*, 13360.
40. Strop, P., and Mayo, S. L. (2000) Contribution of surface salt bridges to protein stability. *Biochemistry 39*, 1251.
41. Makhatadze, G. I., Loladze, V. V., Ermolenko, D. N., Chen, X.-F., and Thomas, S. T. (2003) Contribution of surface salt bridges to protein stability: Guidelines for protein engineering. *J. Mol. Biol. 327*, 1135.
42. Horovitz, A., Serrano, L., Avron, B., Bycroft, M., and Fersht, A. R. (1990) Strength and cooperativity of contributions of surface salt bridges to protein stability. *J. Mol. Biol. 216*, 1031.
43. Lassila, K. S., Datta, D., and Mayo, S. L. (2002) Evaluation of the energetic contribution of an ionic network to β-sheet stability. *Protein Sci. 11*, 688.
44. Spector, S., Wang, M., Carp, S. A., Robblee, J., Hendsch, Z. S., Fairman, R., Tidor, B., and Raleigh, D. P. (2000) Rational modification of protein stability by the mutation of charged surface residues. *Biochemistry 39*, 872.
45. Marshall, S. A., Morgan, C. A., and Mayo, S. L. (2002) Electrostatics significantly affect the stability of designed homeodomain variants. *J. Mol. Biol. 315*, 189.
46. Lee, K. K., Fitch, C. A., and García-Moreno, E. B. (2002) Distance dependence and salt sensitivity of pairwise, coulombic interactions in a protein. *Protein Sci. 11*, 1004.
47. Luisi, D. L., Snow, C. D., Lin, J.-J., Hendsch, Z. S., Tidor, B., and Raleigh, D. P. (2003) Surface salt bridges, double-mutant cycles, and protein stability: an experimental and computational analysis of the interaction of the Asp23 side chain with the N-terminus of the N-terminal domain of the ribosomal protein L9. *Biochemistry 42*, 7005.
48. Langsetmo, K., Fuchs, J. A., and Woodward, C. K. (1989) *Escherichia coli* thioredoxin folds into two compact forms of different stability to urea denaturation. *Biochemistry 28*, 3211.
49. Georgescu, R. E., Garc×c1a-Mira, M. D. M., Tasayco, M. L., and Sánchez-Ruiz, J. M. (2001) Heat capacity analysis of oxidized *Escherichia coli* thioredoxin fragments (1−73, 74−108) and their noncovalent complex. Evidence for the burial of apolar surface in protein unfolded states. *Eur. J. Biochem. 268*, 1.
50. Marley, J., Liu, M., and Bracken, C. (2001) A method for efficient isotopic labeling of recombinant proteins. *J. Biomol. NMR 20*, 71.
51. Mori, S., Abeygunawardana, C., Johnson, M. O., and van Zijl, P. C. M. (1995) *J. Magn. Reson. 108*, 94.
52. Delaglio, F., Grzesiek, S., Vuister, G. W., Zhu, G., Pfeifer, J., and Bax, A. D. (1995) NMRPipe: a multidimensional spectral processing system based on UNIX pipes. *J. Biomol. NMR 6*, 277.
53. Johnson, B. A., and Blevins, R. A. (1994) NMRView: A computer program for the visualization and analysis of NMR data. *J. Biomol. NMR 4*, 603.
54. Koradi, R., Billeter, M., and Wüthrich, K. (1996) MOLMOL: A program for display and analysis of macromolecular structures. *J. Mol. Graphics 14*, 51.
55. Bashford, D., and Gerwert, K. (1992) Electrostatic calculations of the pK_a values of ionizable groups in bacteriorhodopsin. *J. Mol. Biol. 224*, 473.
56. Sanner, M. F., Olson, A. J., and Spehner, J.-C. (1996) Reduced surface: An efficient way to compute molecule surfaces. *Biopolymers 38*, 305.
57. Tasayco, M. L., and Chao, K. (1995) NMR study of the reconstitution of the β-sheet of thioredoxin by fragment complementation. *Proteins: Struct. Funct. Genet. 22*, 41.
58. Chandrasekhar, K., Krause, G., Holmgren, A., and Dyson, H. J. (1987) Assignment of the ^{15}N NMR spectra of reduced and oxidized *E. coli* thioredoxin. *FEBS 284*, 178.
59. Vaughan, C. K., Harryson, P., Buckle, A. M., and Fersht, A. R. (2002) A structural double-mutant cycle: estimating the strength of a buried salt bridge in barnase. *Acta Crystallogr., Sect. D: Biol. Crystallogr. 58*, 591.
60. Horovitz, A. (1996) Double-mutant cycles: a powerful tool for analyzing protein structure and function. *Folding Des. 1*, R121.
61. Gómez, J., Hilser, V. J., Xie, D., and Freire, E. (1995) The heat capacity of proteins. *Proteins 22*, 404.
62. Kraulis, P. J. (1991) MOLSCRIPT: A program to produce both detailed and schematic plots of protein structures. *J. Appl. Crystallogr. 24*, 946.
63. Merritt, E. A., and Bacon, D. J. (1997) Raster3D photorealistic molecular graphics. *Methods Enzymol. 277*, 505.

BI0354684